Fire Technology

Manufactured in The United States
https://doi.org/10.1007/s10694-022-01263-w

Improving Heat Flux Predictions for Directional Flame Thermometers by Incorporating Convective Effects

Juliette I. Franqueville, Jan-Michael Cabrera and Ofodike A. Ezekoye, Mechanical Engineering Department, University of Texas at Austin, Austin, TX 78712, USA*

Received: 22 October 2021/**Accepted:** 16 April 2022

Abstract. The directional flame thermometer (DFT) is a device used to measure radiative heat flux in fire scenarios. In many DFT applications, radiation is the dominant mode of heat transfer and convection does not significantly affect radiative heat flux predictions. However, at higher air velocities, neglecting convection causes error in heat flux predictions. This study explores the error caused by ignoring forced convection in heat flux predictions and proposes a method to reduce it. To accomplish this, a forward heat transfer model is used to generate synthetic temperature data for the DFT given radiative and convective conditions. Using the forward model and an existing inverse model, this study shows that assuming natural convection is the only mode of convective heat transfer leads to significant error in the predicted radiative heat flux. To reduce this error, this work proposes a framework for recovering the heat transfer coefficient and radiative heat flux in forced convection conditions. The framework utilizes an additional thermocouple above the plate of the DFT. The framework performed poorly for simulations in which the temperature of the air stream and that of the thermocouple was lower than 15°C. Omitting simulations where this condition holds, on average, using the framework under constant heat flux and constant characteristic air velocity conditions reduces the error in the predicted heat flux by a factor of 12 compared to when the heat flux is predicted assuming that natural convection is the only mode of convection. A simple experimental test was conducted to validate the computational framework.

Keywords: Heat flux sensors, Directional flame thermometers, Radiative heat flux, Convectiveheat flux

1. Introduction

Directional flame thermometers (DFTs) are robust sensors designed to measure heat flux in fire environments. Typical DFTs are built using two Inconel or stainless steel plates which sandwich a layer of ceramic fiber insulation material. ASTM E3057 [1] outlines the typical DFT design and data analysis process. Inverse models such as those developed by Cabrera et al. [2], Beck Engineering Consultants [3], or Sandia National Laboratories [4] are used to solve for the

*Correspondence should be addressed to: Ofodike A. Ezekoye, E-mail: dezekoye@mail.utexas.edu

Published online: 11 May 2022

radiative heat flux incident on a DFT using the temperature measurements from the two plates.

In many fire applications, radiation is the dominant mode of heat transfer, and convection is often overlooked or ignored. However, in scenarios where gas velocity is significant (for example, in fires affected by crosswinds [5] or in small shallow furnaces [6]), careful characterization of convection is necessary to obtain accurate heat flux measurements. Convection is also significant when the DFT temperature differs from the surrounding gas temperature; for example, in the measurement locations where air entrained into the fire is cooler than the DFT.

In the literature, convection is handled in various ways. For example, Keltner et al. [7] and Sultan [8] ignore convection in their heat flux inversions. In both cases, they note that this approximation is valid for quasi-steady conditions (after 5–10 min) when the temperature of the air and that of the front plate of the DFT are close. However, in the early stages of their tests, the heat flux is under-predicted due to neglecting convection. In their work, Kokel et al. [9, 10] assume that convection heat transfer is characterized by mixed (both forced and free) convection with an assumed characteristic air velocity of 0.5 m/s for tests run in a laboratory environment. In room fire tests, they neglect forced convection while noting that this approximation is a source of error in their predictions. Lam and Weckman [5] test DFTs with a cone calorimeter in conditions varying from natural to forced convection. They use a heat gun that propels a stream of air with velocities ranging from 0 to approximately 8 m/s and use natural and forced convection correlations as appropriate to estimate the heat transfer coefficient for each flow condition. They note that their heat flux measurements are improved when taking thermocouple air temperature measurements instead of assuming a standard value of 22°C.

The literature presented shows that ignoring convective heat transfer limits the application of DFTs to locations where convection is minimal (usually the ground) or to quasi-steady conditions. If convective heat transfer can be characterized by natural convection only, the heat transfer coefficient can be relatively easily estimated using natural convection correlations utilizing the Rayleigh number. In mixed or forced convection conditions, characterization of flow velocity combined with the use of correlations proves to be useful. However, flow velocity is very difficult to estimate in fire environments.

This work shows the conditions under which ignoring forced convection causes significant error when recovering radiative heat flux incident on a DFT. Then, a framework consisting of adding an additional thermocouple on top of the typical DFT design to estimate the heat transfer coefficient in forced convection conditions is proposed. The range of conditions for which the proposed method works is also discussed. Although the framework is primarily tested using synthetic data, an experimental test is conducted where the DFT used corresponds to the design developed by Cabrera et al. [2].

2. Method

2.1. Simulation Setup for Investigating the Importance of Convection

First, the conditions under which ignoring forced convection causes significant error when recovering radiative heat flux incident on a DFT are explored. Temperature data are generated using a forward model. An incident radiative heat flux is specified on the front plate of the DFT with a "top hat" profile typical of tests run using a cone calorimeter. An air flow velocity for a stream of air flowing over the front plate of the DFT, u, is specified, as well as the temperature of the surroundings and that of the stream of air. Figure 1 shows the setup.

The heat flux and the stream of air are assumed to only affect the front plate of the DFT. The governing equation for the front plate of the DFT is:

$$\rho_s c_s L_f \frac{dT_f}{dt} = q''_{inc} - q''_{refl,f} - q''_{conv,f} - q''_{emit,f} - q''_{cond,f} \tag{1}$$

Where q''_{inc} is the incident radiation on the DFT, $q''_{refl,f}$ is the reflected portion of the radiative heat flux, $q''_{conv,f}$ is the convective heat flux, $q''_{emit,f}$ is the emitted radiation, and $q''_{cond,f}$ is the heat flux lost to the insulation layer. Using the appropriate expressions for the heat flux terms, the following equation is obtained:

$$\rho_s c_s L_f \frac{dT_f}{dt} = \alpha_s q''_{inc} - h_f(T_f - T_\infty) - \varepsilon_s \sigma(T_f^4 - T_{sur}^4) - q''_{cond,f} \tag{2}$$

The heat transfer coefficient on the front plate, h_f, depends on the prescribed velocity u as well as the convection regime (natural, mixed, or forced convection). For laminar natural convection, the following correlation is used (with parameters 0.65 and 1/4 taken from [2]):

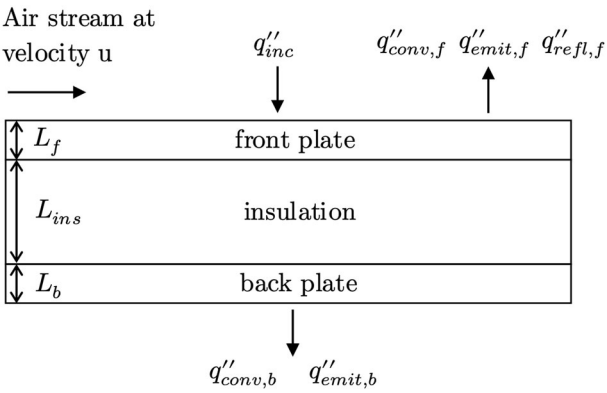

Figure 1. Figure showing the DFT setup. The front plate is exposed to a stream of air at velocity *u* and to an incident heat flux.

$$\overline{Nu} = 0.65Ra^{\frac{1}{4}} \tag{3}$$

Where Ra, the Rayleigh number, is:

$$Ra = \frac{g\beta_{air}(T - T_\infty)L^3}{v_{air}\alpha_{air}} \tag{4}$$

$\overline{Nu}$, the Nusselt number, is equal to $\overline{h_f}L_s/k_{air}$, where L is the length of the DFT plates. For laminar forced convection, the following correlation is used:

$$\overline{Nu} = 0.664Re_L^{\frac{1}{2}}Pr^{\frac{1}{3}} \tag{5}$$

Re is the Reynolds number which is equal to uL/v_{air}, where u is the prescribed velocity. If $Gr/Re^2 \ll 1$ (where Gr is the Grashof number), it is assumed that forced convection is the dominant mode of convective heat transfer. If $Gr/Re^2 \gg 1$, natural convection is dominant. If $Gr/Re^2 \sim 1$, both forced and natural (''mixed'') convection are considered. In this case, the Nusselt number is equal to:

$$\overline{Nu}^3_{mix} = \overline{Nu}^3_{natural} + \overline{Nu}^3_{forced} \tag{6}$$

Where $\overline{Nu}^3_{natural}$ and $\overline{Nu}^3_{forced}$ are evaluated using equations 3 and 5, respectively. Given the prescribed conditions, the ''true'' heat transfer coefficient, h_f, is derived from the Nusselt number calculated using equation 3 for natural convection, equation 5 for forced convection, or equation 6 for mixed convection.

For the insulation layer, the governing differential equation is:

$$\rho_{ins}c_{ins}\frac{\partial T_{ins}}{\partial t} = k_{ins}\frac{\partial^2 T_{ins}}{\partial x^2} \tag{7}$$

The governing equation for the back plate of the DFT is similar to that of the front plate:

$$\rho_s c_s L_b \frac{dT_b}{dt} = -h_b(T_b - T_\infty) - \varepsilon_s\sigma(T_b^4 - T_{sur}^4) + q''_{cond,b} \tag{8}$$

Where $q''_{cond,b}$ is the heat flux gained from the insulation layer by conduction. It is assumed that the air stream only affects the front plate, so the relevant mode of convection on the back plate is natural convection. Equation 3 is used to derive h_b. The boundary conditions for the system of differential equations are:

$$q''_{cond,f} = -k_{ins}\left.\frac{\partial T}{\partial x}\right|_{x=0} \tag{9}$$

$$q''_{cond,b} = -k_{ins} \left. \frac{\partial T}{\partial x} \right|_{x=L_{ins}} \tag{10}$$

and at $t = 0$, all temperatures are equal to T_{sur}. The three governing equations are integrated numerically to generate synthetic temperature data. The insulation layer is split into finite volumes and the temperatures are computed at each node. Material properties are evaluated at the initial DFT temperature according to correlations presented in [2]. The dimensions of the DFT used in the simulations correspond to the design developed by [2].

To explore the conditions under which convection is significant, synthetic temperature data are generated using the forward model given various conditions. For all simulations, the simulation time is 10 min. From 0 to 3 min, the heat flux is 0, the air temperature is 21°C, and the air velocity is 0. From 3 min to 8 min, a constant heat flux, a constant air velocity, and a constant air temperature are prescribed. From 8 min until 10 min, the heat flux returns to 0, the air temperature returns to 21°C, and the air velocity returns to 0.

70 incident heat fluxes ranging from 5 kW/m^2 to 150 kW/m^2 are tested. Although typical heat fluxes in post-flashover compartments range from 70 kW/m^2 to 150 kW/m^2 , heat fluxes as low as 5 kW/m^2 are also of interest as critical heat fluxes for secondary ignition may be this low [11]. 10 velocities ranging from 0.1 m/s to 15 m/s are tested. Although velocities in compartment fires are on the lower end of this range, velocities outdoors can be 10 m/s and higher. 35 air temperatures ranging from 21°C to 1000°C are tested; this range was chosen because 1000°C is a typical temperature for a post-flashover compartment fire [12]. All tested values are linearly spaced. All possible combinations are tested, so in total, $70 \times 10 \times 35 = 24500$ simulations are run. Note that not all combinations may be representative of a real scenario, but all were tested for comprehensiveness.

The aim is to determine the error caused by neglecting forced convection. For each simulation, temperature profiles as a function of time for the two DFT plates and the finite volume nodes of the insulation layer are obtained. These temperature distributions are used to recover the prescribed heat flux. Here, the inverse model developed by Cabrera et al. [2] is used. Details about this model can be found in their work; however, a brief explanation of how the model works is given here. The inputs for the inverse model are the temperatures of the front and back plates of the DFT, the material properties, and the heat transfer coefficients for the two plates. In typical experiments, the plate temperatures are measured by thermocouples placed on the two plates. Here, the two temperature inputs correspond to the temperatures of the front and back plates of the DFT generated using the forward model, T_f and T_b. Then, the inverse model uses equation 7 with $T_{ins}(x = 0, t) = T_f$ and $T_{ins}(x = L_{ins}, t) = T_b$ as boundary conditions to solve for the spatial-temporal temperature of the insulation layer. Using a control volume on the entire DFT gives the following energy balance:

$$q''_{st,tot} = q''_{inc} - q''_{refl,f} - q''_{emit,f} - q''_{conv,f} - q''_{emit,b} - q''_{conv,b} \tag{11}$$

Where $q''_{st,tot}$ is the total energy stored per unit area. All terms on the right hand side of the equation are easily determined using T_f, T_b, material properties, and heat transfer coefficients. The energy stored per unit area in the front and back plates is determined from the derivatives with respect to time for T_f and T_b. The energy stored per unit area in the insulation layer is obtained by applying energy conservation to the insulation layer. The energy stored per unit area is equal to the energy flowing into the insulation minus that flowing out: $q''_{st,ins} = q''_{in,ins} - q''_{out,ins}$, where

$$q''_{in,ins} = -k_{ins} \left. \frac{\partial T_{ins}}{\partial x} \right|_{x=0} \tag{12}$$

and

$$q''_{out,ins} = -k_{ins} \left. \frac{\partial T_{ins}}{\partial x} \right|_{x=L_{ins}} \tag{13}$$

Which are calculated using the spatial-temporal temperature of the insulation layer previously derived. With all terms known, q''_{inc} can be determined.

Instead of using the inverse model with the "true" heat transfer coefficient (h_f) used when generating the synthetic temperature data, it is assumed that the only mode of convection is natural convection when using the inverse model to recover the prescribed heat flux. To calculate the natural convection heat transfer coefficient, the natural heat transfer correlation (equation 3) is used regardless of whether the true convection mode is natural, mixed, or forced convection. For each simulation, the inverse model is used to recover the prescribed heat flux with the synthetic temperature data generated using the "true" h_f and the natural convection coefficient, $h_{f,nat}$, as inputs. Note that when $Gr/Re^2 > 1$, $h_f = h_{f,nat}$.

For each simulation, the prescribed heat flux, the heat flux recovered using the true heat transfer coefficient (which allows for checking that it is almost identical to the prescribed heat flux), and the heat flux recovered using the natural convection heat transfer coefficient are recorded. The mean percentage error between the heat flux initially prescribed and the heat flux recovered using the natural convection heat transfer coefficient is also recorded. Additionally, the time-averaged convective heat transfer per unit area in each simulation, $h_f(T_f - T_\infty)$, is recorded. In the results section, the relationship between the mean percentage error mentioned above and the mean convective heat transfer per unit area is explored.

Figure 2 illustrates the process for one simulation. Figure 2(a) shows the temperature profiles for the front and back DFT plates for $q''_{inc} = 9$ kW/m^2, $T_\infty = 80$ °C and $u = 3.4$ m/s. $u = 3.4$ m/s corresponds to an average heat transfer coefficient of 26 W/m^{2}K. In this case, the average convective heat transfer on the front plate of the DFT is 2.5 kW/m^2. Figure 2(b) shows the prescribed incident heat flux and the heat fluxes recovered using the actual heat transfer coefficient and natural convection only heat transfer coefficient. Here, the average percentage

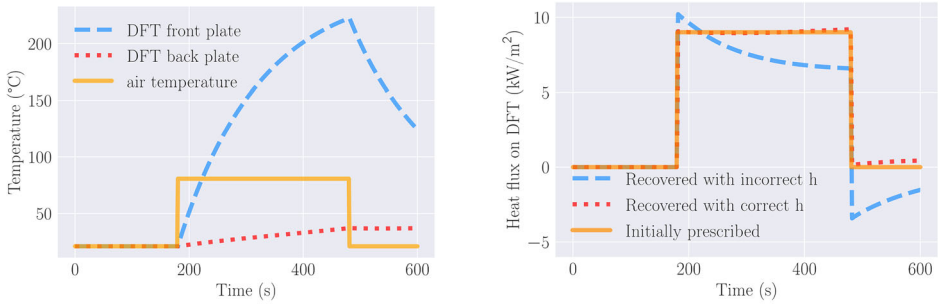

(a) (b)

Figure 2. (a) Temperature profiles for $q''_{inc} = 9$ kW/m², $T_\infty = 80$°C and $u = 3.4$ m/s (b) Prescribed incident heat flux, and heat fluxes recovered using the actual heat transfer coecient and natural convection only heat transfer coecient.

error between the heat flux recovered using the natural heat transfer coefficient and the heat flux initially prescribed is 20%.

2.2. Framework for Estimating the Heat Transfer Coefficient in Forced Convection Conditions

Next, a framework for estimating the heat transfer coefficient in forced convection conditions is proposed. In this case, the forward model described above is modified to account for an additional thermocouple attached to the front plate of the DFT and exposed to the stream of air flow. In short, the thermocouple adds an additional equation to the inverse problem, and assuming that the incident heat flux and characteristic velocity on the thermocouple and the DFT are the same allows to solve for the true heat transfer coefficient, and therefore give a better estimate of the incident heat flux.

The proposed setup is shown in Figure 3.

The thermocouple is modeled as a lumped sphere. It is assumed that the incident radiative heat flux, q''_{inc}, is the same on the thermocouple and the front plate of the DFT. It is also assumed that the velocity of the stream of air adjacent to the thermocouple and the front plate of the DFT is the same. The governing equations for the DFT (equations 2, 7 and 8) are unchanged, but an additional equation for the thermocouple is introduced:

$$\rho_{TC} V_{TC} c_{TC} \frac{dT_{TC}}{dt} = A_{TC}(q''_{inc} - q''_{refl} - q''_{conv,TC} - q''_{emit,TC}) \tag{14}$$

or

$$\frac{1}{3}\rho_{TC} c_{TC} R_{TC} \frac{dT_{TC}}{dt} = \alpha_{TC} q''_{inc} - h_{TC}(T_{TC} - T_\infty) - \varepsilon_{TC}\sigma(T_{TC}^4 - T_{sur}^4) \tag{15}$$

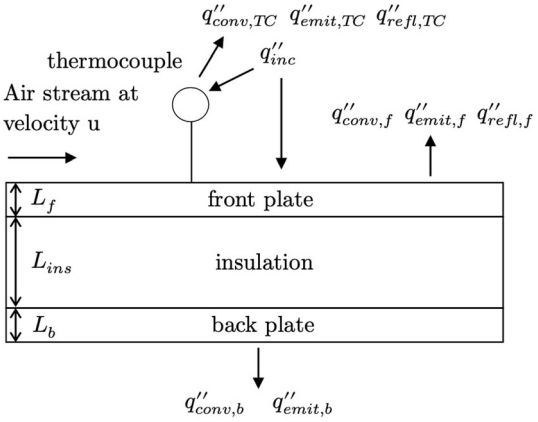

Figure 3. Figure showing the DFT setup for the framework. The front plate of the DFT and the thermocouple are exposed to a stream of air at velocity *u* and to an incident heat flux.

The heat transfer coefficient for the thermocouple is calculated using the following forced convection correlation [13]:

$$\overline{Nu} = 2 + (0.4Re_D^{\frac{1}{2}} + 0.06Re_D^{\frac{2}{3}})Pr^{0.4}\left(\frac{\mu_\infty}{\mu_s}\right)^{\frac{1}{4}} \tag{16}$$

Where $Nu = \overline{h_{TC}}D/k$. All properties are evaluated at T_∞ except for μ_s which is evaluated at surface temperature. Thermal conductivity, specific heat capacity, and density for a K-type thermocouple given by [14] are used in the simulations. Additionally, an emissivity of 0.8 is assumed as done in [15]. All properties are assumed to be constant with temperature. Using the equations for the DFT and the equations for the thermocouple described above, synthetic data for the DFT and the thermocouple are generated.

Then, the following process is used to recover the forced convection heat transfer coefficient and predict the incident heat flux on the DFT more accurately. First, an air stream velocity u is guessed for each time step. Then, using the initial guess for u, the forced convection correlation for the heat transfer coefficient for the top plate of the DFT (equation 5) is used to derive the DFT heat transfer coefficient at each time step, h_f. Using h_f and the temperature of the top plate of the DFT generated using the forward model with a prescribed velocity, incident heat flux, and air and surroundings temperature, the model described in [2] is used to recover the incident heat flux on the DFT. Using the energy balance described in equation 15 and synthetic temperature data for the thermocouple (obtained for the same conditions as for the DFT), the heat transfer coefficient for the thermocouple is found. Then, using the correlation given in equation 16, Re_D is found using a numerical root-finding method. From Re_D, the updated u is found. This process is repeated until u and the incident heat flux on the DFT converge. Note

that the quantities above are vectors of the same length as the number of time steps in the synthetic temperature data. Figure 4 illustrates the process.

Alternatively, the process described above can be run using a more rigorous optimization algorithm (Powell's method, available in SciPy in Python). In this case, a function which takes in the velocity vector u and returns a mean squared error as a measure of misfit is defined. Using the forced convection correlations for the DFT and the thermocouple, h_f and h_{TC} are calculated. Then, using h_f and the inverse model described in [2], the incident heat flux on the DFT is calculated. Separately, using h_{TC} and equation 15, the incident heat flux on the thermocouple is calculated. Since these two heat fluxes should be equal, their mean squared error is calculated. The optimization algorithm then finds the vector u for which the mean squared error is minimized. Although both approaches gave very similar results, the former ran faster and was therefore preferred.

The forward model is used to generate synthetic temperature data for conditions typical of cone calorimeter tests where a "top hat" incident heat flux is specified and the velocity of the air flow is constant in time. Using the framework described above, the heat transfer coefficient and radiative heat flux are recovered. This process is repeated for conditions representative of real tests where the prescribed heat flux, the velocity, and the air temperature are transient. Additionally, this work explores which range of conditions the recovered incident heat flux is significantly improved compared to when a natural convection heat transfer coefficient is used regardless of the convection mode.

2.3. Experimental Setup

Preliminary experiments were conducted to validate the proposed framework. An ASTM E1354 cone calorimeter was used to produce the required incident heat flux on the DFT. The cone was configured so that the heat flux on the DFT was 10 kW/m^2. The ambient temperature was 21°C. The DFT used followed the design of Cabrera et al. [2]; a thorough explanation of the DFT design can be found in their manuscript. The DFT was attached to a ring stand and placed underneath the heating element at the appropriate distance. A thermocouple was placed above the DFT as shown in Figure 5. A fan was also attached to the ring stand. Temperature data for the two DFT thermocouples and the additional thermocouple were taken using a Graphtec GL840 midi logger with a 0.5 second sampling period.

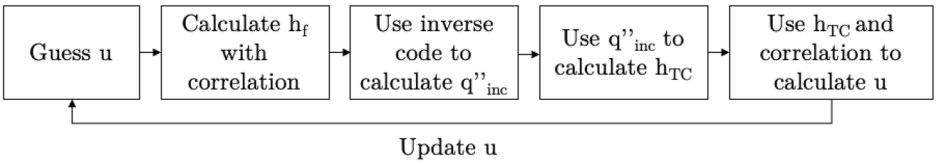

Figure 4. Flowchart showing the process for recovering the forced convection heat transfer coefficient and the incident radiative heat flux.

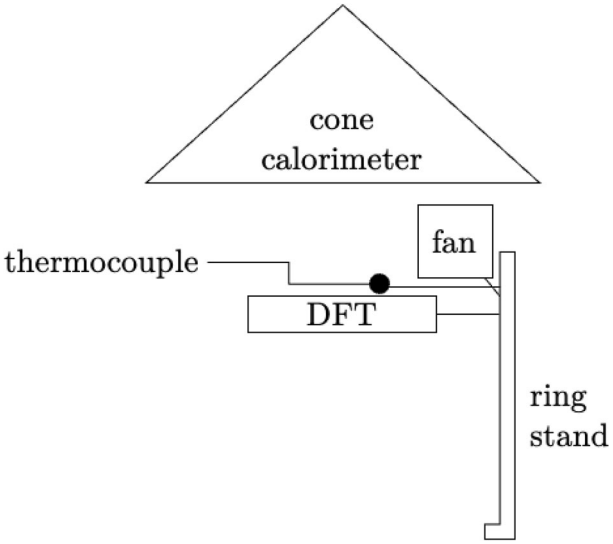

Figure 5. Diagram showing the experimental setup. In the first test, the fan was turned off.

For the first test, the fan was turned off, so the DFT was not exposed to forced convection. For the second, the fan was turned on to create an air stream over the front plate of the DFT. The total test time was 10 min. The heating element shutters were opened from 3 to 8 min.

3. Results and Discussion

3.1. Estimating Error Generated Due to Natural Convection Assumption

As outlined in the methodology section, the error associated with assuming that convection heat transfer occurs by natural convection only is determined. Figure 6 shows the results from the 24500 simulations run. In (a), each point represents one simulation, where the horizontal axis shows the mean convective heat flux for each simulation and the vertical axis shows the mean percentage error obtained in the radiative heat flux recovered under the natural convection only assumption. The points are colored according to their corresponding radiative heat flux. In (b), the data are collapsed by dividing the mean convective heat flux by the radiative heat flux.

Figure 6(a) shows that the error in the recovered radiative heat flux increases more sharply for smaller prescribed heat fluxes. This can be attributed to the fact that for small heat fluxes, $h\Delta T$ represents a large percentage of the radiative heat flux compared to when radiative heat fluxes are high. For each radiative heat flux, the error appears to increase linearly with convective heat transfer. Figure 6(b) shows that the data collapse when the mean convective heat transfer is divided by the radiative heat flux. As expected, as the ratio of convective to radiative heat

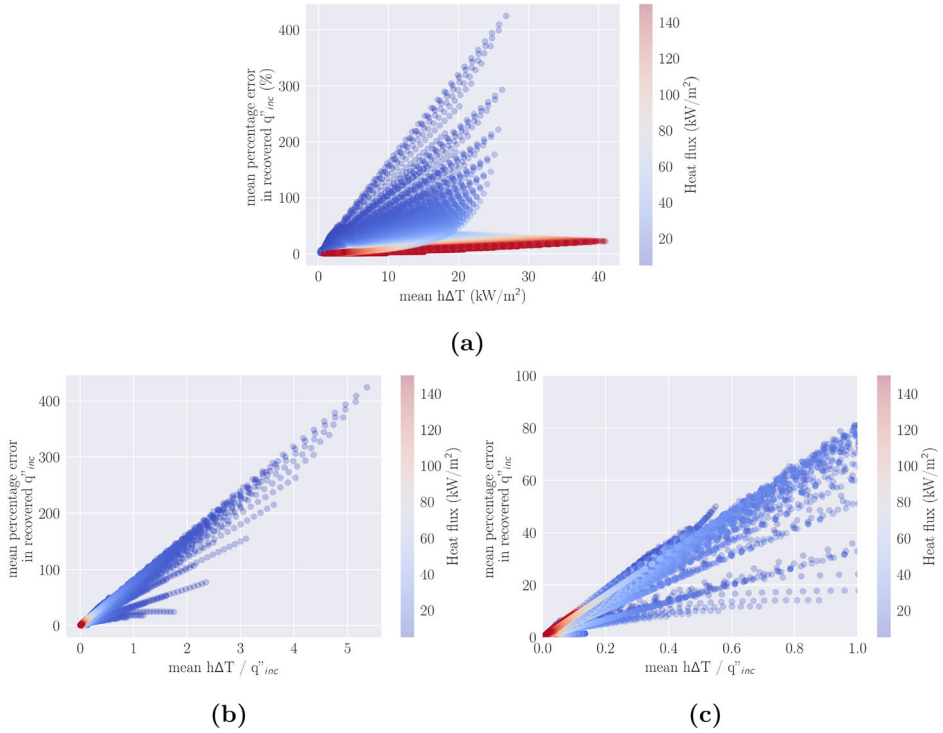

Figure 6. (a) Plot showing the mean percentage error in the recovered radiative incident heat flux averaged over time against the mean convective heat flux, also averaged over time for radiative heat fluxes ranging from 5 to 150 kW/m² (b) Plot showing the mean percentage error in the recovered radiative incident heat flux averaged over time against the ratio of convective to radiative heat transfer (c) A close-up plot of (b).

transfer increases, the error in the recovered heat flux increases. The error becomes significant ($>10\%$) when $h\Delta T/q''_{inc}$ is larger than 0.1, and goes as high as approximately 400% as the ratio increases. The points which have very low error correspond to simulations for which the prevalent mode of convection is natural convection. Figure 6(c) shows a close up view of Figure 6(b). Although most points with high prescribed heat fluxes have negligible error, at high velocities the error for high heat fluxes is still significant. For the highest heat flux, 150 kW/m^2, the error goes as high as 22% when the velocity is 15 m/s.

The plots highlight the need to accurately characterize convection when it is a significant mode of heat transfer. If the error threshold required is 10%, for example, the natural convection assumption may not be acceptable if the average $h\Delta T/q''_{inc}$ is higher than 0.1. In the next section, the framework developed is used to estimate the heat transfer coefficient under forced convection conditions and reduce the error in the recovered radiative heat flux.

3.2. Recovering Incident Heat Flux Under Simple Conditions

The previous section showed that ignoring forced convection when it is significant leads to large errors in the predicted heat flux. The goal of this section is to evaluate how well the proposed framework reduces these errors. One heat flux (10 kW/m^2) and ambient temperature (21°C) combination is chosen from the previous section for this analysis. For this heat flux and ambient temperature, the framework is tested for 3 linearly spaced velocities (2, 4 and 6 m/s). The radiative flux for these cases is first recovered without the framework (using the natural heat transfer coefficient $h_{f,nat}$) and then using the framework. It should be noted at the start of the simulations where no incident heat flux is imposed (before 3 min), the temperatures of the DFT and the thermocouple are equal to T_∞. At the end of the simulations (after 8 min), the temperature of the thermocouple quickly drops to T_∞. When the difference between the air stream temperature and that of the thermocouple and/or that of top plate of the DFT is zero, it is impossible for the framework to recover the forced heat transfer coefficient because any coefficient would give zero convective heat flux given that $\Delta T = T - T_\infty = 0$. As a result, the forced heat transfer coefficient is only recovered for time steps where the heat flux is imposed. At the start of the simulation, the same heat transfer coefficient as the one recovered at the first time step where the heat flux is imposed is used. For the end of the simulation, the same heat transfer coefficient as the one recovered at the last time step where the heat flux is imposed is used.

Figure 7 shows the prescribed incident heat flux and the convective heat flux, as well as the recovered heat fluxes when the heat transfer coefficient is derived from the natural convection correlation (a through c) and when the framework is used (d through f). The mean squared error (MSE) between the prescribed and recovered incident (radiative) heat fluxes are noted in the figure. As expected, the mean squared error increases as velocity increases when natural convection only is assumed (sub-figures a through c). Sub-figures d through f show that the proposed framework reduces the mean squared error by as much as a factor of 25 times compared to when natural convection only is assumed. The error in the recovered heat flux is low regardless of the prescribed velocity. Figure 8 shows the true forced heat transfer coefficients and the ones recovered using the framework, which correspond to sub-figures d through f in Figure 7. The mean squared errors between the predictions and the "true" heat transfer coefficients vary from 0.5 to 1.5 W/m^2 K.

3.3. Recovering Incident Heat Flux Under Transient Conditions

The steps above are repeated, but this time for conditions more representative of real fire tests. A transient incident heat flux of t-squared form is specified, where the starting flux is 0 and the maximum is 10 kW/m^2. A transient air temperature of t-squared form ranging from 21 to a maximum of 70°C at the end of the simulation is also specified. Additionally, linearly increasing or decreasing velocities are specified. As in the previous section, three velocity curves are tested; the line coefficients for each velocity curve are chosen using a random number generator.

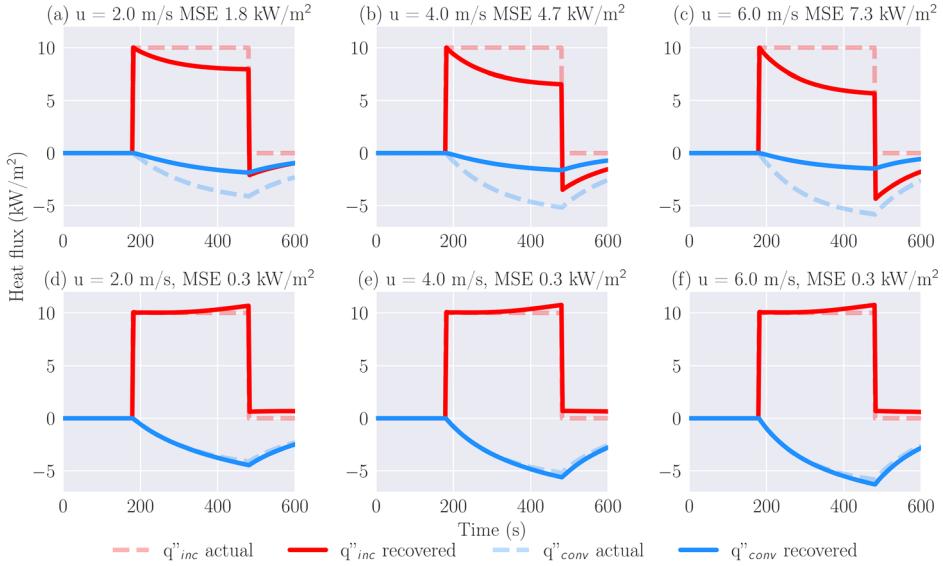

Figure 7. Figure showing the prescribed incident heat flux and the convective heat flux, as well as the recovered heat fluxes when the heat transfer coefficient is derived from the natural convection correlation (a through c) and when the framework is used (d through f).

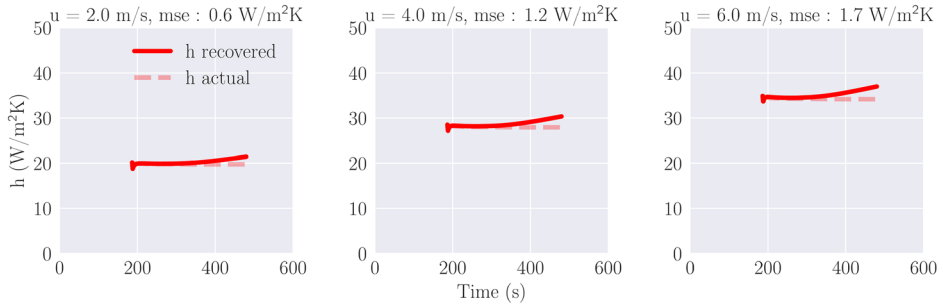

Figure 8. Figure showing the prescribed and recovered forced convection heat transfer coefficients for the recovery framework.

Figure 9 shows the recovered radiative and convective heat fluxes for the three air stream velocity curves when natural convection only is assumed (a through c). Note that the velocities given in the figure are the average of the time-dependent velocity for each simulation. The mean squared error values are slightly lower than in the cases shown in the previous section given that T_∞ is higher, making convection less significant. Figures 9 d through f shows the recovered heat flux when the framework is used. As before, the framework significantly reduces the mean squared error in the predicted radiative and convective heat fluxes. The

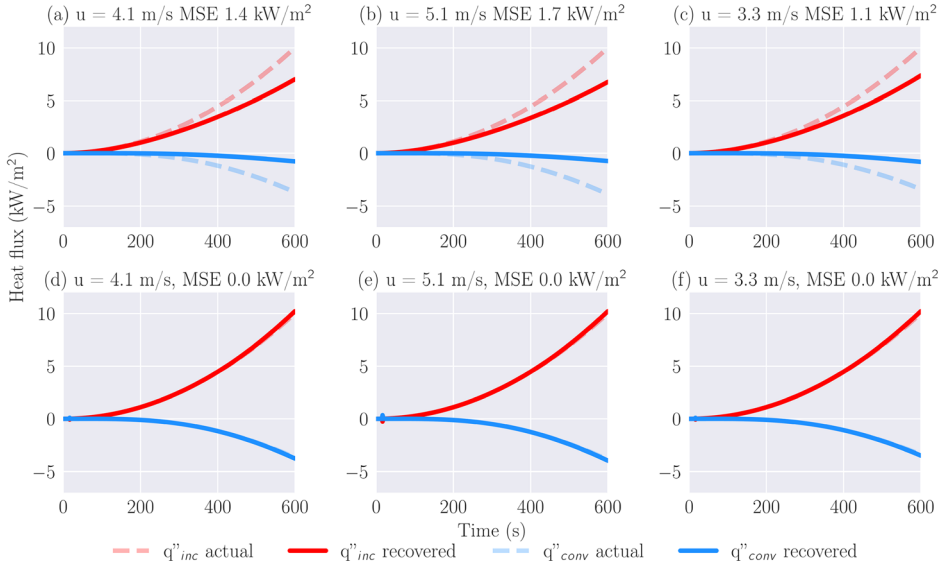

Figure 9. Figure showing the prescribed incident heat flux and the convective heat flux, as well as the recovered heat fluxes when the heat transfer coefficient is derived from natural convection only (a through c) and when the framework is used (d through f) for three prescribed velocity curves.

mean squared error values between the prescribed and recovered heat fluxes for the cases shown are almost negligible.

Figure 10 shows the prescribed and recovered heat transfer coefficients for the DFT corresponding to cases d through f. The mean squared error between the "true" and recovered heat transfer coefficient varies from 0.3 to 0.4 kW/m^2 K. Here, the radiative heat flux is prescribed throughout the simulation; therefore, it

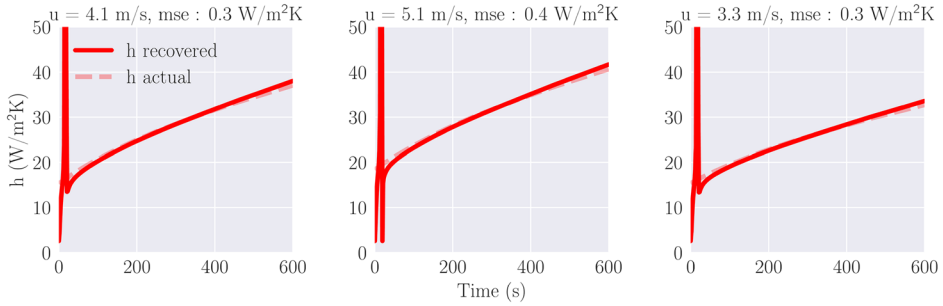

Figure 10. Figure showing the prescribed and recovered forced convection heat transfer coefficients for the recovery framework. Note that the first two time steps were removed from the mean squared error calculation.

is possible to recover the heat transfer coefficient and radiative heat flux for almost all time steps. At the very start of the simulations, however, the system is in thermal equilibrium and the framework is unable to recover the heat transfer coefficient because there is almost no heat transfer; this can be seen in Figure 10. Despite causing a large error in the recovered heat transfer coefficient, this issue does not significantly affect the recovered heat flux.

3.4. Comparison with Natural Convection Assumption

This section compares the error in the predicted heat flux obtained if the framework is used to the error obtained when the heat flux is recovered using the natural convection heat transfer coefficient. The same data presented in Sect. 3.1 are used, but here the heat flux is recovered both using the natural convection heat transfer coefficient and the heat transfer coefficient recovered using the framework. Note that the framework is tested on all points, but in reality, at low convective to radiative heat flux, the framework may not be necessary given that the natural convection assumption leads to low error.

When testing the framework on all points, a significant number of points still showed high error in the recovered heat flux. Figure 11 helps identify under which conditions the framework did not perform well. Note that the framework was considered to perform poorly for a recovered heat flux error of 10% and above, so the error cutoff in Figure 11 is 10%. However, points may have larger error than this. The plot shows error as a function of air temperature and radiative heat flux. Note that each point is averaged across velocities. This was done because the plot did not significantly change across velocities. To illustrate this, the same plot is provided in Figure 12 for a 5 m/s velocity and a 15 m/s velocity.

As mentioned before, the framework works poorly when the temperature of the thermocouple is close or equal to the air temperature. Plotting the average differ-

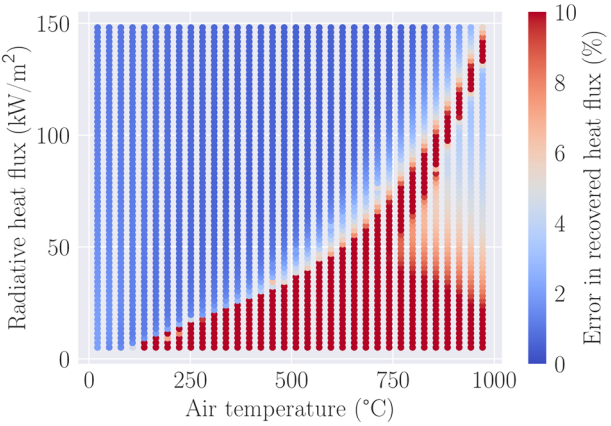

Figure 11. Plot showing the error in the recovered heat flux as a function of air temperature and radiative heat flux. The error is averaged across velocities.

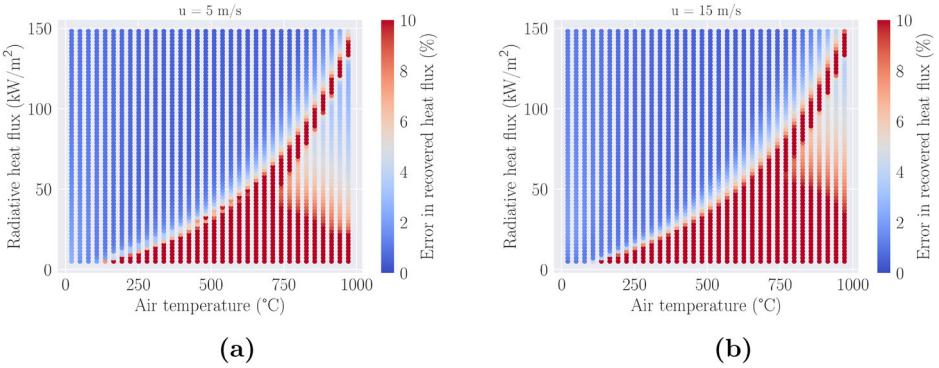

Figure 12. (a) Plot showing the error in the recovered heat flux as a function of air temperature and radiative heat flux when the air velocity is 5 m/s (b) Plot showing the error in the recovered heat flux as a function of air temperature and radiative heat flux when the air velocity is 15 m/s.

ence between the thermocouple and air temperatures for each simulation (again averaged across all velocities) reveals that the points corresponding to an error higher than 10% correspond to simulations where the average difference between the thermocouple and air temperatures is less than 15°C. This plot is shown in Figure 13.

Additionally, when generating synthetic temperature data for the DFT and the thermocouple, natural, mixed and forced convection are considered. However, the framework is used to recover the radiative heat flux for all cases where $Gr/Re^2 < 1$

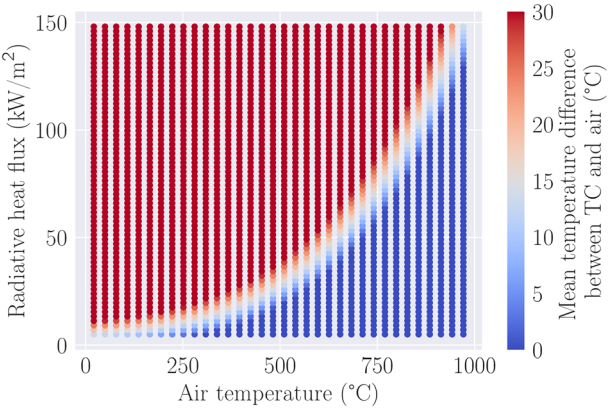

Figure 13. Plot showing the mean difference between the thermocouple and air temperature as a function of heat flux and air temperature. Differences are averaged across all velocities. Note that the difference cutoff was set to 30°C to better observe the similarities in this figure and Figure 11.

but otherwise a natural convection heat transfer coefficient is used. The mixed region where $Gr/Re^2 \approx 1$ is not considered, which is an additional source of error for points lying in this region.

Figure 14 shows the same plots as Figure 6 where the vertical axis shows the mean percentage error in the recovered heat flux and the horizontal axis shows the mean convective heat flux for (a), and the ratio of the mean convective heat flux to the radiative heat flux for (b). Each point represents one simulation. The data in red are identical to the data shown in Sect. 3.1, and the data in blue show the error in the recovered heat flux obtained using the framework. When using the framework to recover heat flux, it should be noted that if the average Gr/Re^2 over a simulation is larger than 1 (which indicates that natural convection is prevalent), the appropriate natural convection heat transfer coefficient is used to recover the incident heat flux rather than the framework.

Note that given the discussion above, the framework was only used on simulations for which to average temperature difference between the thermocouple and air was larger than 15°C. Using this filter, 67% of the simulations were kept and the rest does not appear in Figure 14. In practice, one would need to know the ambient air temperature to be able to determine whether the average temperature difference between the thermocouple and air is larger than 15°C. This can be achieved using shielded thermocouples.

Figure 14(a) shows that as the convective heat flux increases, the framework significantly reduces the error in the recovered heat flux. On average, the ratio of the error for the "assuming natural convection" points to the error for the "using framework" points is 12. For 99.6% of simulations, the error in the recovered heat flux is brought down to below 10%, with the exception of a couple points at low convective heat flux. These points can be eliminated by setting the threshold

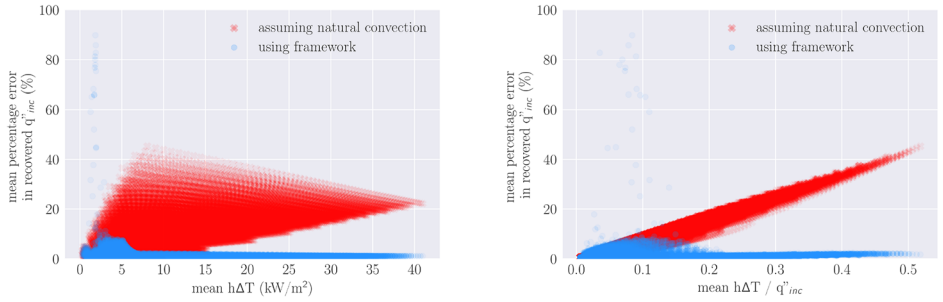

Figure 14. (a) Plot showing the mean percentage error in the recovered radiative incident heat flux averaged over time against the mean convective heat flux when natural convection only is assumed and when the framework is used. (b) Plot showing the mean percentage error in the recovered radiative incident heat flux averaged over time against the ratio of convective to radiative heat transfer for both cases.

in difference between thermocouple and air temperature to 20°C instead of 15°C. In practice, since these points occur at low convective heat transfer, it is best to assume natural convection.

3.5. Experimental Results

Figure 15 shows the sampled temperatures for the thermocouples attached to the DFT and the additional thermocouple for the two tests: the first test without fan and the second with fan. Note that the temperature of the additional thermocouple is not shown for the no-fan case because it is not relevant in the analysis.

For the no-fan test, the unmodified inverse code, which uses a natural convection correlation to estimate the heat transfer coefficient, was used. For the fan test, both methods were used: assuming natural convection and using the framework presented in this manuscript. Note that the additional thermocouple temperature was smoothed using a Savitzky-Golay filter (available in the Python package Numpy) prior to using the framework.

Figure 16 shows the recovered heat fluxes. The data were smoothed for clarity. As expected, the unmodified inverse code is able to predict the heat flux well for

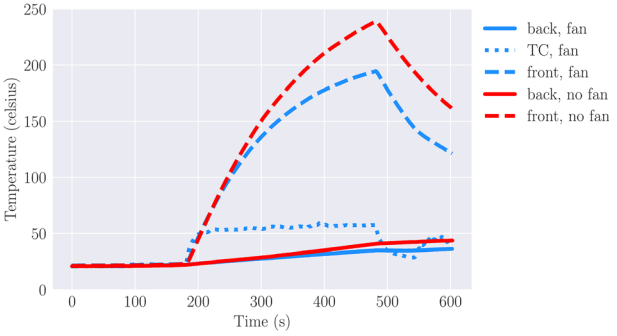

Figure 15. Plot showing temperature data for the two tests.

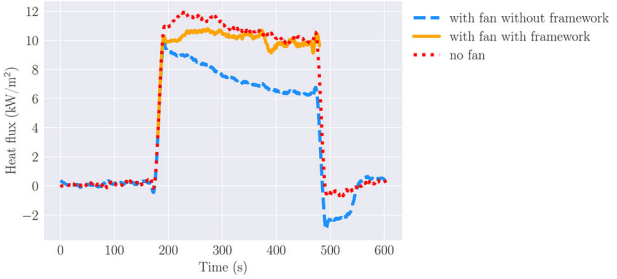

Figure 16. Plot showing recovered heat flux for the test without fan (assuming natural convection, red) and for the test with fan (assuming natural convection, blue and using framework, orange).

the case where the fan is turned off. For the fan test, the unmodified inverse code does not predict the heat flux accurately; the mean percentage error with the prescribed heat flux is 25% (or 4.8 kW/m^2 mean squared error). Note that the heat flux was not recovered when the heating element was turned off because as explained above, the framework cannot solve for the heat transfer coefficient when the air and thermocouple temperatures are too close. Using the proposed framework reduces the mean percentage error to 11% (or 7.94 kW/m^2 mean squared error). Although the errors are larger than with synthetic data, the mean percentage error is divided by a factor of 2.3 when using the framework and the mean squared error is divided by 3.9.

4. Conclusion

This work showed that ignoring convection or assuming that natural convection is the only mode of convection in DFT heat flux measurements can lead to significant error at high convective heat flux. This limits the use of DFTs to areas where convection is not significant; for example, the ground, or to when experiments have reached a quasi-steady state. Using a modified design for the DFT where a thermocouple is placed on top of the DFT plate can significantly reduce the error in heat flux predictions under forced convection conditions. To show this concept, temperature data for the DFT and the thermocouple were simulated using a forward heat transfer model. Using forced convection heat transfer coefficient correlations and an existing inverse model, the framework utilizes an iterative process to recover the heat transfer coefficient and radiative heat flux on the DFT. This framework was tested for simple conditions characteristic of tests run using a cone calorimeter and reduced the mean squared error in heat flux predictions by a factor of 25 compared to when it was assumed that natural convection only is significant. Additionally, this framework was tested for conditions representative of real experiments, where the heat flux, air velocity, and ambient temperature are transient. The error in the recovered heat flux for these cases was low. Lastly, for 24,500 simulations, the heat flux predictions made using the framework were compared to predictions made with the assumption that natural convection only is significant. The framework performed poorly when the difference in temperature between the thermocouple and surrounding air was lower than 15°C. Omitting the simulations where this condition was met, the framework divided the percentage error in the predicted heat flux by an average factor of 12. A preliminary experiment was also run using a cone calorimeter and showed that the framework reduced error by a factor of 2.3.

Acknowledgements

This work is supported by U.S. National Science Foundation under Award No. 1707090.

Author Contributions

JIF: Methodology, software, formal analysis, visualization, writing—original draft.OAE: conceptualization, methodology, funding acquisition, supervision,writing—review and editing.JMC: conceptualization, methodology, writing—review and editing.

Declarations

Conflict of interest The authors declare that they have no known competing financial interests or personalrelationships that could have appeared to influence the work reported in this paper.

References

1. ASTM (2019) Standard test method for measuring heat flux using directional flame thermometers with advanced data analysis techniques. Tech. Rep., ASTM
2. Cabrera J, Moser R, Ezekoye O (2020) A modified directional flame thermometer: development, calibration, and uncertainty quantification. J Verif Valid Uncertain Quantif 5(03):011003
3. Beck J (1999) User's manual for ihcp1d: program for calculating surface flux from transient temperatures inside solids. Beck Engineering Consultants Co, Okemos, MI
4. Blackwell B, Douglass R, Wolf H (1990) Soddit. sandia one-dimensional direct and inverse thermal code. Tech. rep., Sandia National Labs, Albuquerque, NM
5. Lam C, Weckman E (2009) Steady-state heat flux measurements in radiative and mixed radiative-convective environments. Fire Mater Int J 33(7):303–321
6. Sultan M (2010) Comparisons of temperature and heat flux in furnaces controlled by different types of temperature sensors. In: Parker AJ (ed) Advances in the state of the art of fire testing ASTM International, West Conshohocken
7. Keltner N, Beck J, Nakos J (2010) Using directional flame thermometers for measuring thermal exposure. J ASTM Int 7(2):1–12
8. Sultan M (2010) Performance of different temperature sensors in standard fire resistance test furnaces. Fire Technol 46(4):853–881
9. Philip K (2008) Modeling of directional flame thermometer for real-time incident radiation measurements in room fire testing. Master's thesis, The University of Texas at Austin
10. Kokel P, Weinschenk C, Ezekoye O (2010) Evaluation of directional flame thermometer for real-time inversion of heat flux. Int Heat Transf Conf 49392:83–92
11. Drysdale D (2011) An introduction to fire dynamics. Wiley, New York
12. Kutz M (2018) Handbook of environmental degradation of materials. William Andrew, Norwich
13. Whitaker S (1972) Forced convection heat transfer correlations for flow in pipes, past flat plates, single cylinders, single spheres, and for flow in packed beds and tube bundles. AIChE J 18(2):361–371
14. Kazemi M, Nobes D, Elliott J (2017) Effect of the thermocouple on measuring the temperature discontinuity at a liquid-vapor interface. Langmuir 33(28):7169–7180

15. Roberts I, Coney J, Gibbs B (2011) Estimation of radiation losses from sheathed thermocouples. Appl Therm Eng 31(14–15):2262–2270